



Full Length Article

Displacement dynamics of trapped oil in rough channels driven by nanofluids

Yuanhao Chang^a, Senbo Xiao^{a,*}, Rui Ma^a, Xiao Wang^b, Zhiliang Zhang^a, Jianying He^{a,*}

^a NTNU Nanomechanical Lab, Department of Structural Engineering, Norwegian University of Science and Technology (NTNU), 7491 Trondheim, Norway

^b School of Materials Science and Engineering, China University of Petroleum (East China), Qingdao, 266580 Shandong, China



ARTICLE INFO

Keywords:

Enhanced oil recovery
Displacement mechanism
Nanoparticles
Trapped oil
Molecular dynamics

ABSTRACT

It is well accepted that nanofluids have great potential in enhanced oil recovery (EOR). However, the EOR mechanisms by nanofluids largely remain elusive. In the study, the displacement dynamics of residual oil trapped in rough channels by different nanofluids under varied injection pumping forces are investigated by atomistic modeling. Our results indicate that both hydrophilic nanoparticles (NPs) and Janus NPs have highly obvious oil displacement effects. Specifically, hydrophilic NPs increase the viscosity and enlarge the sweeping scope of injected fluid, while Janus NPs favor either staying at the oil–water interface to reduce the interfacial tension or adsorbing onto the convex surface. Under the drag of the injecting flux, Janus NPs displace trapped oil molecules and alter the local surface wettability by sliding along the surface. In contrast, hydrophobic NPs are prone to migrate into the oil phase, which not only reinforces the trapping effect of the oil molecules by the rough surface but also poses a risk of channel blockage. Despite that the oil displacement effect of all the injection fluids is found to be less significant with low pumping force, the Janus NPs are able to maintain a stable oil displacement performance under low pumping force thanks to their sufficiently long contact time with the oil phase. Furthermore, analysis on capillary number indicates that Janus NPs have outstanding application potentials in reservoirs under realistic flooding conditions. Our findings provide atomistic insights into the mechanism of nanofluids in EOR and shed light on the selection and optimization of NPs.

1. Introduction

Being the most widely used fossil fuel in the world, petroleum is the most important raw material in the modern industrial society [1,2]. The aggressive exploration of petroleum via primary and secondary oil recovery has exhausted most of the oil fields global wide. Currently, there are urgent calls for new technologies of tertiary oil recovery, i.e. the enhanced oil recovery (EOR), for extracting the residual and more than 60% of the original oil in place (OOIP) [3,4]. There are mainly three types of conventional EOR methods, namely thermal methods, gas injection, and chemical flooding [5]. Despite the ample research devoted to the thermal methods and gas injection, the corresponding applications are yet limited due to the harsh reservoir adaptation conditions and low economic benefits [6,7]. The traditional EOR methods also encounter many challenges of high energy and chemicals cost and formation damage [8,9]. Recently, EOR with nanofluids has attracted great attention and interest, thanks to the application potentials of nanoparticles (NPs), especially the high efficiency at low cost and their

compatibility with environmental protection [10–12].

Compared with traditional chemical flooding ingredients, NPs have obvious advantages in improving both sweep efficiency and displacement efficiency. On the one hand, their small size allows them to transport into the small channels. On the other hand, their high surface energy and reactivity are conducive to modify the properties of fluids and rock surfaces, thereby improving oil displacement [13,14]. So far, NPs have achieved highly encouraging results in both laboratory and field experiments [12]. There are multiple NPs-enabled EOR mechanisms proposed, including interfacial tension reduction [15], wettability alteration [16–18], viscosity adjustment [19,20], pore channel plugging [21], and appearance of structural disjoining pressure [22–25]. Depending on specific experimental parameters (NPs properties, core properties, flooding rate, residual oil, etc.), different mechanisms may dominate EOR [26]. The multiple mechanisms proposed also indicate that EOR by NPs is a complex process, with many nanoscale behaviors remaining unclear. More fine-scale work is in desire for elucidating the mechanism of various NPs under different reservoir conditions.

* Corresponding authors.

E-mail addresses: senbo.xiao@ntnu.no (S. Xiao), jianying.he@ntnu.no (J. He).

<https://doi.org/10.1016/j.fuel.2021.122760>

Received 1 July 2021; Received in revised form 21 November 2021; Accepted 28 November 2021

Available online 4 December 2021

0016-2361/© 2021 The Author(s). Published by Elsevier Ltd. This is an open access article under the CC BY license (<http://creativecommons.org/licenses/by/4.0/>).

Molecular dynamics (MD) simulations have been proven to be extremely effective tools for revealing the fundamentals of EOR mechanisms [27–29]. Firstly, MD simulations are able to decipher the key interactions among the chemical agent and oil and water that are key to the understanding of the EOR mechanism. MD simulations have been utilized to systematically unravel the interfacial activities and molecular interactions between crude oil components (mainly asphaltenes) and different types of surfactants [30–34]. For NPs specifically, MD simulations are widely used for clarifying their interfacial behaviors and characteristics in oil–water systems studied [25,35–37]. Moreover, MD simulation can provide nanoscale dynamics of NPs in oil trapping channels and the underlying mechanisms of nanofluids in EOR, which is challenging to monitor with current experimental capability.

There are notable atomistic investigations considering the effects of rock surface properties on the transportation of NPs in the confined channels using MD simulations. Wu et al. simulated the flow behavior of nanofluids in confined clay channels filled with oil [38]. Wang et al. studied the spreading of nanofluids and the detachment process of the oil droplet [39,40]. Wang et al. investigated the imbibition and displacement mechanism of NPs transportation [41–43]. The reported simulations were however all based on smooth channels, which cannot fully reflect the flow characteristics of nanofluids on rough rock surfaces in the reservoir [44–47]. Apparently, the motion pattern and the roles of NPs in EOR in the rough channel are different from the ideally smooth surface adopted in the previous studies. Furthermore, the displaced phase in previous studies consisted of only pure oil phase, which cannot present the residual oil distribution in most channels in the EOR period.

To reveal the realistic displacement dynamics of trapped oil, MD simulations of injecting various nanofluids into rough channels were carried out in this work, aiming to elucidate the EOR mechanisms enabled by different NPs (hydrophilic, hydrophobic, and Janus NPs). The displacement phenomena of trapped oil driven by nanofluids were compared, with the specific role of each NP type in EOR uncovered. Moreover, the influence of the injection driving force underlying the EOR effect is clarified. The results rationalize the basis of the EOR mechanism by NPs and provide guidance of NPs optimization in petroleum engineering.

2. Model and simulation details

2.1. Model systems

The aim of the modeling is to uncover the effects and mechanisms on the displacement of trapped oil in rough channels by nanofluids. Even at the nanoscale, such a system might require scales in length and time

beyond the limit of all-atom modeling. For example, a single nanoparticle with a diameter of 5 nm already contains thousands of atoms, which needs an extremely large amount of computer resources for the corresponding simulations. In order to build a sufficiently large system containing a good number of nanoparticles, and at the same time achieve a meaningful time scale of oil displacement, approximations in the interatomic potentials are critically important. As such, coarse-grained model systems including inlet, channel, and outlet parts were constructed to feature injection of nanofluids in the EOR process, as shown in Fig. 1. For the sake of simplicity, all the model systems were built as semi-2D with a width of 25.34 Å in the y-axis (Fig. 1). The boundary conditions applied in the systems were periodic. The channel part contained residual oil/water/rough surfaces, mimicking the important characteristics of channels in the oil reservoir. The rough surface in the system consisted of pillars separated by even intervals, as dimensions given in Fig. 1. With the given hydrophobicity of the surface (atomistic parameters given in the following text), residual oil was trapped on the rough surface structure of the channel after primary water flooding. The detailed process to obtain the channel part with residual oil was given in the supporting information S1. The channel block in Fig. 1 consisted of 939 oil molecules and 9482 water molecules in total, with a volume size of $200.97 \times 25.34 \times 120.82 \text{ \AA}^3$.

The inlet of the systems included the displacing phase and the piston, with a length of 181.95 Å in the injection direction. There were four kinds of displacing phases: water (NP-free) and three types of nanofluids (with fifty hydrophilic, hydrophobic, or Janus NPs). The density of oil and water was correspondingly kept as 659 kg/m^3 and 1003 kg/m^3 , which are in excellent agreement with their experimental values [48,49]. The rough surfaces and NPs shared the same diamond cubic crystalline lattice structure with a lattice constant of 5.43 Å. The diameter of NPs was 7 Å. With the 50 NPs in each nanofluid, the NPs volume concentration was $\sim 1.73\%$ in the systems. To enable the injection of the nanofluids into the channel, a piston was placed on the left side of the displacing phase (Fig. 1). The driving force was applied on the piston to mimic the applied pressure. The piston had the same cross-section area of the channel and a thickness of 10.86 Å, which was larger than the cutoff distance (10 Å) of non-bonded interactions to avoid mutual interference of possible interactions on both sides of the piston. The outlet part was built as the buffering space at the exit of the channel, and initially had a length of 50.12 Å as indicated in Fig. 1.

The choice of atomistic interaction parameters was the same as in the former study [25]. The mW water model was chosen for the water phase, while the Transferable Potentials for Phase Equilibria united-atom (TraPPE-UA) description of hexane was used for oil [49,50]. The coarse-grained mW water model is famous for its accuracy, including

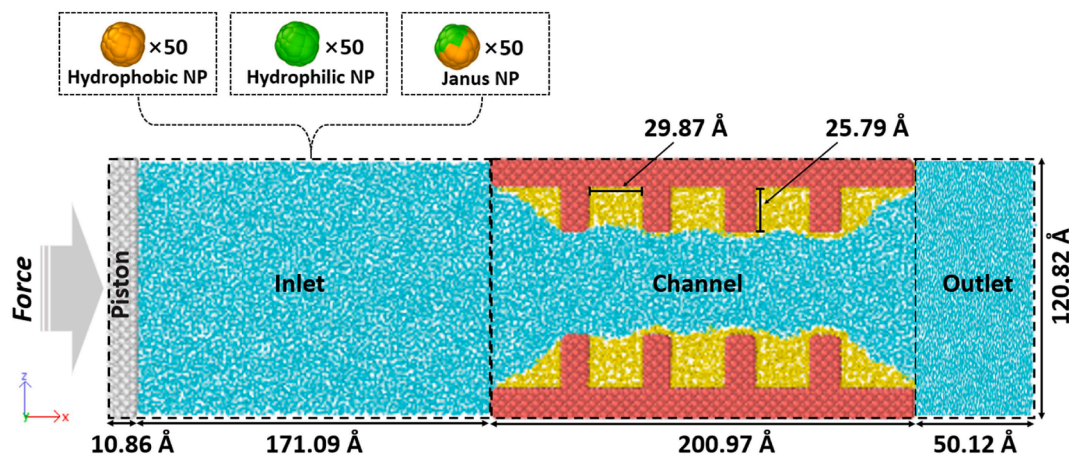


Fig. 1. Representative of model systems containing inlet, channel, and outlet parts. The colors for different phases: piston (grey), water (cyan), rough surface (red), oil (yellow), hydrophobic NP (orange), hydrophilic NP (green), Janus NP (orange and green). The grey arrow indicates the direction of the applied force. (For interpretation of the references to colour in this figure legend, the reader is referred to the web version of this article.)

featuring hydrogen bonding, at less than 1% of the computational cost of other all-atom water models, while the TraPPE-UA force field has outstanding performances in realizing the appropriate properties of phase equilibrium of different materials, especially alkanes including hexane. The interaction of the water model mW followed the form of the Stillinger–Weber potential:

$$E = \sum_i \sum_{j>i} \varphi_2(r_{ij}) + \sum_i \sum_{j\neq i} \sum_{k>j} \varphi_3(r_{ij}, r_{ik}, \theta_{ijk}) \quad (1)$$

$$\varphi_2(r_{ij}) = 7.049556277\epsilon \left[0.602245584 \left(\frac{\sigma}{r_{ij}} \right)^4 - 1 \right] \exp\left(\frac{\sigma}{r_{ij} - 1.8\sigma} \right) \quad (2)$$

$$\varphi_3(r_{ij}, r_{ik}, \theta_{ijk}) = 1.2\epsilon [\cos\theta - \cos 109.47^\circ]^2 \exp\left(\frac{1.2\sigma}{r_{ij} - 1.8\sigma} \right) \exp\left(\frac{1.2\sigma}{r_{ik} - 1.8\sigma} \right) \quad (3)$$

with characteristic interaction size $\sigma = 2.3925 \text{ \AA}$, and characteristic energy $\epsilon_{ww} = 6.189 \text{ kcal/mol}$. The pairwise non-bonded interactions in TraPPE-UA followed the Lennard-Jones (LJ) potential:

$$U_{LJ} = 4\epsilon_{ij} \left[\left(\frac{\sigma_{ij}}{r_{ij}} \right)^{12} - \left(\frac{\sigma_{ij}}{r_{ij}} \right)^6 \right] \quad (4)$$

where the energy well depths for oil-oil and oil–water were $\epsilon_{oo} = 0.0914 \text{ kcal/mol}$ and $\epsilon_{ow} = 0.1191 \text{ kcal/mol}$, respectively. A characteristic energy well ϵ_{so} of 0.2 kcal/mol was given to the surface–oil interaction to enable the hydrophobic characteristic of the surfaces, as details provided in Fig. S2. A weak interaction 0.01 kcal/mol was applied between the piston and other types of molecules to minimize the influence of the piston on the flooding process. The overall interaction potentials between the NPs were provided in Table S1 [43]. All the atoms in the systems were free of charge.

2.2. Computational details

The LAMMPS package was adopted to carry out all the simulations [51]. First, all the systems were energy-minimized using the steepest descent method and then equilibrated for 3 ns in the NVT ensemble using a simulation timestep of 3 fs. It should be noted here that the timestep with coarse-grained models like the mW coarse-grained water can be up to 10 fs [49,50,52]. In order to conserve the total energy of a large system stably and save the calculation costs, a timestep of 3 fs was chosen for all the simulations in this work. The temperature was controlled at 300 K by the Nosé–Hoover thermostat with a damping coefficient of 100 fs [53,54]. As can be seen from Fig. S3, the total

potential energy of the systems quickly reached a plateau in the equilibration. For enabling nanofluid injection, a constant force of $10^{-4} \text{ kcal/mol/\AA}$ along the x-axis was applied on the piston, as depicted in Fig. 1. The displacement process in each simulation ended as the whole injected fluid volume was pushed into the channel, namely the piston was in close contact with the channel. The NPs were treated as rigid bodies to maintain the spherical shape. Meanwhile, the rough surfaces were fixed in position to speed up the simulation process. Ovito software was employed for the visualization and analysis [55].

3. Result and discussion

3.1. Displacement process

3.1.1. Displacement phenomenon

The surface properties of NPs determined their transportation behaviors, which subsequently influenced the displacement of the trapped oil. As the snapshots of the displacement process at different stages shown in Fig. 2, the trapped oil was partially moved toward the outlet section by different extent as time increased in all the systems, including the reference NP-free system. In all the nanofluids, different types of NPs entered and passed through the rough channels efficiently from 0.6 to 2.3 ns. Nevertheless, there were differences in the behavior patterns of the three NPs during the displacement. Particularly, Janus NPs were more likely to adsorb at the oil–water interface or stay near the top of the pillars, while most hydrophobic NPs were prone to enter and stay inside the oil, forming aggregated clusters. All the hydrophilic NPs stayed in the injected water phase, with the majority being displaced out of the channeling along with oil molecules.

The trapped oil in the four systems was displaced in different amounts by nanofluids. To further evaluate the flooding efficiency, residual oil molecules in the channel were recorded as shown in Fig. 3. In all the systems, the total amount of trapped oil molecules in the channel started to show a decreasing pattern at 1.5 ns and maintained such a trend to the end of the simulations (Fig. 3(a)). By comparing the number of oil molecules in the channel at the end of the simulations, the hydrophilic NPs had the best displacement effect (853 oil molecules left), followed by the Janus NPs (876 oil molecules left). Surprisingly, pure water flooding (905 oil molecules left) showed a better effect than that of the hydrophobic NPs (915 residual oil molecules). In detailing the displacement process, the channel was divided into three regions as indicated in Fig. 3(b), with the change of the oil molecule number plotted in Fig. 3(c). It is known that it is difficult for the trapped oil to be further extracted by pure water after initial water flooding, mainly due to the formation of the fixed water flow channels in reservoirs [56,57].

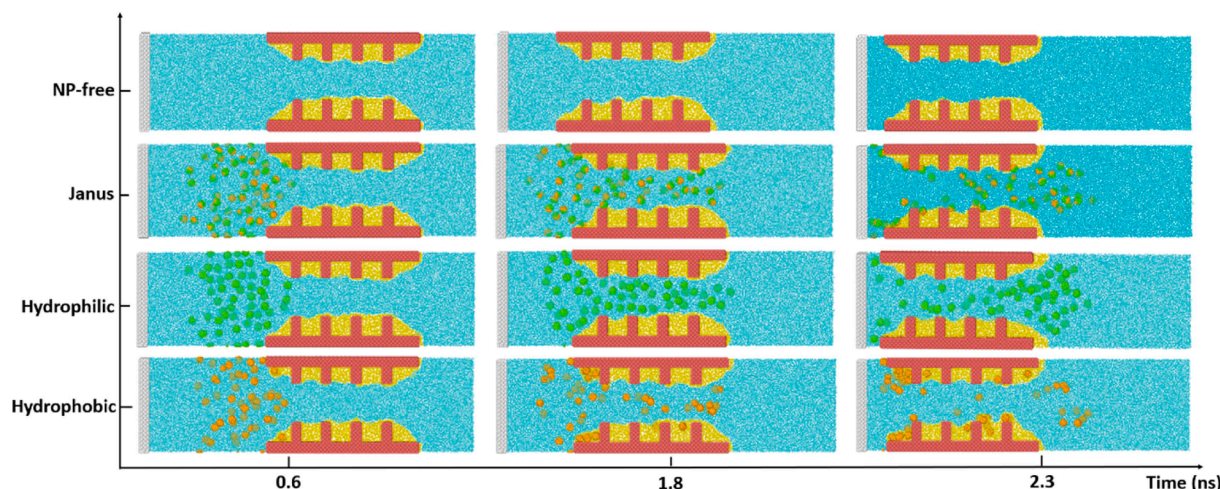


Fig. 2. Representative snapshots of the displacement process in the four systems. The colors for different molecules can be found in Fig. 1.

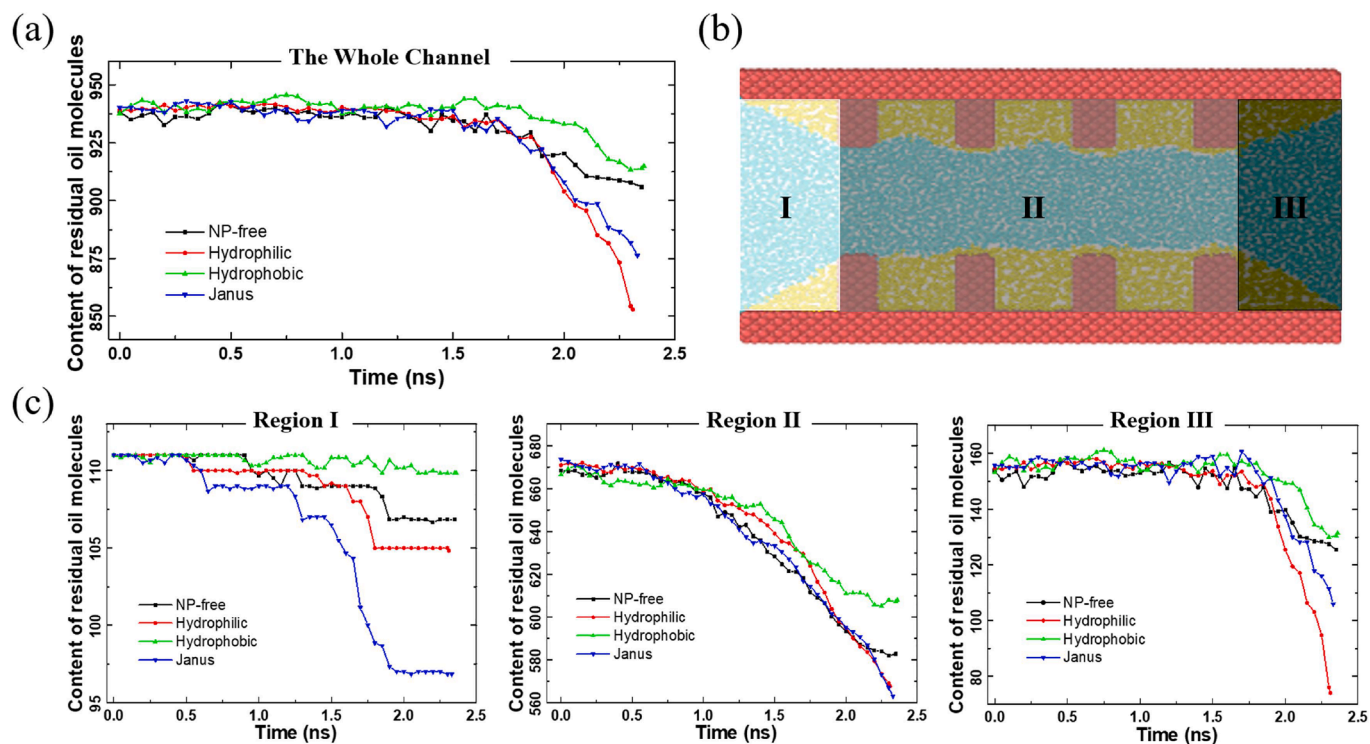


Fig. 3. Displacement of trapped oil in the rough channel. (a) Oil molecules inside the whole channel in the displacement process; (b) The schematic diagram of different regions of the channel for displacement effect comparison; (c) Changes in the number of trapped oil molecules in the three regions of the channel in the displacement process.

Here, the pure water flooding (the NP-free system) still supplied the lateral friction on the trapped oil phase and enabled motions of certain oil molecules close to the oil–water interface. As showed in Fig. 3(c), the displacement effect was observed in each region of the NP-free system, signified by the decreasing number of oil molecules until the end of the simulation. For injection with nanofluids, there were obvious differences in the displacement effect owing to the different properties of NPs, especially in the region I and III as showed in Fig. 3(c). Particularly, nanofluids with Janus and hydrophilic NPs showed a great outperforming displacement effect in the region I and III, respectively. In contrast, injection of hydrophobic NPs yielded the least displaced oil molecules in all three regions of the channel, with nearly no effect at all in region I. This interesting result strongly suggests the application of Janus or hydrophilic NPs in the formulation of nanofluids. The motion

behaviors of different NPs underlying this result were further analyzed in the following.

3.1.2. Flow characteristics of the injection fluids

The atomic velocity of individual trapped oil molecules and the effective flow volume of injection fluids in the channel are the key factors to reflect the EOR effect. Taking the average of continuous 2-ps simulation trajectories with stable injection flux at 2 ns, the distribution of the instant atomic velocity of the oil molecules along the injection direction (velocity along X-axis), was shown in Fig. 4(a). In each case, the instant velocity distribution centered around zero speed. Because of the drag from the injecting flux, all four distributions showed an almost negligible right-skew pattern. Nevertheless, the oil molecules had the highest and the lowest average velocity with hydrophilic and

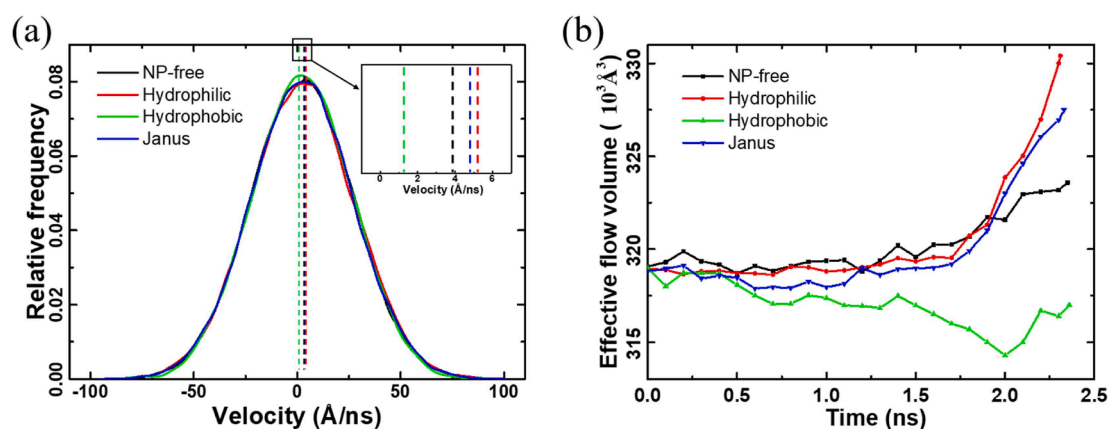


Fig. 4. Flow characteristics of the injection fluids. (a) Atomic velocity distribution of the trapped oil under stable flux in the four systems along the direction of injection. The dotted lines in different colors represent the corresponding average value of the four distributions. (b) The effective flow volume of the injection fluids during the displacement process.

hydrophobic NPs, respectively, as shown by the inset of Fig. 4(a). That is, oil in the hydrophilic case migrated fastest, while the presence of hydrophobic nanoparticles significantly hindered the flow of oil. The collective velocity of oil molecules, namely the total displacement in a certain period normalized by the corresponding time, further clarifies this difference. As shown by the collective velocity of a 20-ps period in Fig. S4, the collective velocity distribution of the oil molecules with the injection of hydrophobic NPs showed a second unique and distinctive peak at low velocity, which can be attributed to the oil molecules tightly bound to the hydrophobic NPs. The properties of the injected NPs indeed had profound effects on the displacement of the trapped oil molecules.

The effective flow volume (V_{flow}) of the injection fluids characterizes the mobile volume of molecules in the channel. The absolute change of V_{flow} is thus approximately equal to the difference between the volume of fluids entering into (V_{in}) and exiting from (V_{out}) the rough channel, namely $\Delta V_{\text{flow}} \approx V_{\text{in}} - V_{\text{out}}$. The ΔV_{flow} quantifies the change in the effective flow volume of the channel during the displacement process, which at the same time determines the difficulty of subsequent fluid injection. As shown in Fig. 4(b), the nanofluids with hydrophilic and Janus NPs, as well as the pure water (NP-free) injections increased the effective flow volume in the rough channel, with the hydrophilic NPs showing the best results. In contrast, the injection of hydrophobic NPs significantly decreased the effective flow volume, meaning it narrows the channel for the injection fluid in the displacement process. That is to say, injection of hydrophobic NPs into rough channels leads to an increase of injection pressure or even blockage of nanopores.

3.2. Mechanism of trapped oil displacement by NPs

The above results indicated that the occurrence of NPs directly affects the oil displacement in the rough channel. In the following sections, the displacement mechanism of different NPs on the trapped oil is analyzed by inspecting the specific micro behaviors of NPs.

3.2.1. Mechanism by hydrophilic NPs

The hydrophilic NPs had led to the best displacement effect on trapped oil. Previous studies indicated that hydrophilic NPs cause the rearrangement of water molecules and affect the diffusion and properties of water molecules [41]. Here, all the hydrophilic NPs were found to disperse in the water phase during the displacement process, as shown in Fig. 2, which suggested that the hydrophilic NPs had altered the properties of the injected fluid. As the comparison of streamlines of water molecules depicted in Fig. 5, the hydrophilic NPs had a significant impact on the dynamics of their neighboring water molecules. In the pure water flooding, the main fluid streamline ran laterally, showing limited disturbances caused by the friction at the oil–water interface. With the occurrence of the hydrophilic NPs, water molecules closely bound to and migrated with the NPs due to the strong interaction forces. The diffusion of the hydrophilic NPs in the nanofluid led to disturbances of the local flow field and deviation of the streamlines from the main flow direction. This resulted in the strong friction to the oil at the

oil–water interface and strengthening of the displacement effect. As the lowest mean square displacement (MSD) of water during the displacement shown in Fig. S5, the hydrophilic NPs obviously impeded water diffusion in the channel if compared with the three other systems. Since the viscosity of the injection fluids was negatively correlated with diffusion speed, the viscosity of the injected water was increased by hydrophilic NPs [58]. Consequently, the mobility ratio (the mobility of displacing fluid divided by that of the displaced fluid) decreased as the viscosity of the injection phase increased [59]. As a result, the sweep efficiency increased, which led to the improvement of the EOR effect.

3.2.2. Mechanism by Janus NPs

In the flooding process, Janus NPs partially dispersed in the water phase and partially adsorbed at the oil–water interface. The impact of Janus NPs on the water diffusion was negligible, as indicated by the MSD results in Fig. S5. It is known that Janus NPs adsorbed at oil–water interfaces modify the interfacial tension [42]. The calculated interfacial tension for oil/water and Janus NPs/oil/water were 56.01 and 49.51 mN/m in this work, as the detailed modeling and calculation method listed in the Supporting information S6, which agreed with the known reduction of interfacial tension [60].

Given their amphiphilic surface properties, Janus NPs were able to strongly interact with different components in the channel, especially with the pillars of the rough solid surface. At the end of the displacement process, the interfaces of oil–solid–water were populated with Janus NPs, as shown in Figs. 2 and 6. Interestingly, Janus NPs actively tangled with the pillar structure and altered the residence of the trapped oil. As the representative snapshots shown in Fig. 6, Janus NPs adsorbed on the backside of the pillar against the injection direction (Fig. 6(a)) in the displacement progresses, and gradually penetrated into the trapped oil along the surface. At the same time, water molecules entered the oil-trapping pocket with Janus NPs and drove the oil molecules outside by volume exclusion. In the process, the NPs migrated inward into the oil-trapping pocket along the solid wall, thanks to the injection flow and the interaction between the NPs and the surface. Meanwhile, the intrusion of water further forced Janus NPs to constantly adjust their orientation on the surface owing to their surface wettability characteristics. Because the hydrophilic parts of Janus NPs were exposed to the fluid, the local wettability of the total surface was thus altered to be more hydrophilic, highly beneficial for oil displacement [61]. Given the higher concentration of Janus NPs and the longer contact in reservoirs, it is expected that the accumulation of more Janus NPs at the three-phase contact area also has the potential to exert the structural disjoining pressure to detach the trapped oil from the surface [23,25].

Janus NPs could also adsorb on the side of pillars facing the injection fluid. In such a situation, the position of Janus NPs was not stable, as illustrated in Fig. 6(b). Driven by the injected fluid, Janus NPs were pushed to slide over the pillars to the backside against the injection. In such a process, oil molecules were mobilized by the NPs, as depicted in Fig. 6 (b) (T1–T5). Similarly, Janus NPs reached the top of the pillars were prone to be pushed forward by flooding, and eventually ended up

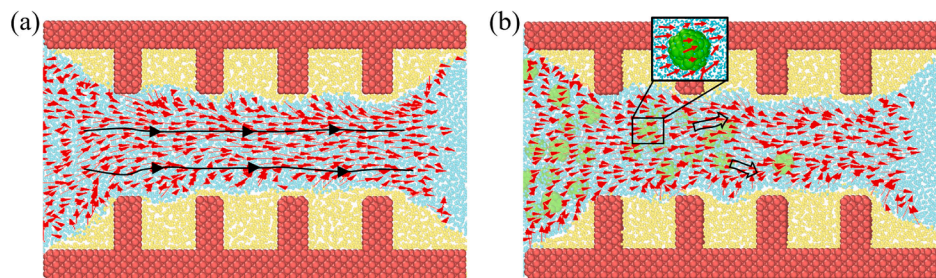


Fig. 5. The streamlines of water at the stable injection state without NPs (a) and with hydrophilic NPs (b). The system snapshots were taken at 1.5 ns, where the injection fluid speed was stable. The black arrows in (a) and (b) showed the average running speed of water molecules for visualization effects. The inset in (b) showed the typical streamline distribution around a certain NP.

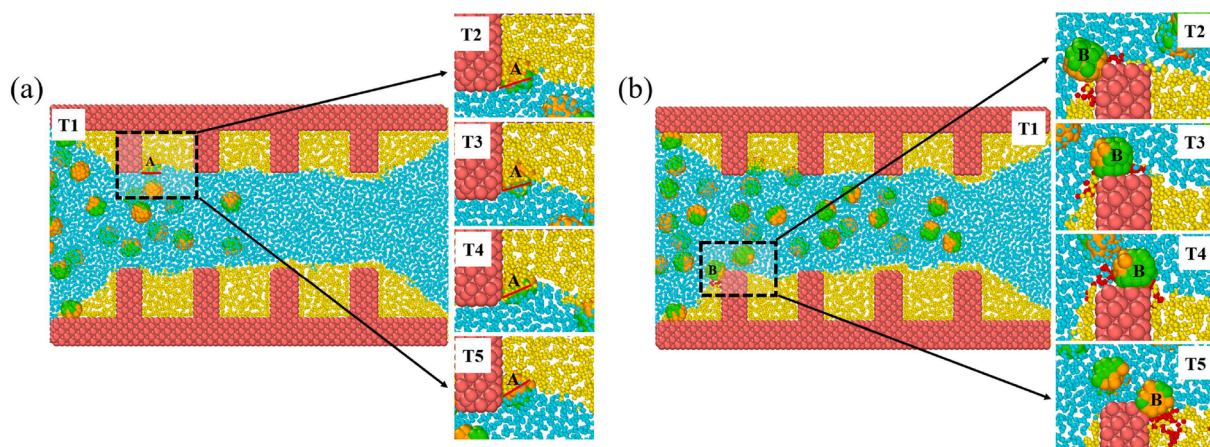


Fig. 6. Migrations of Janus NPs in the channel. (a) A representative Janus NP (marked as A) adsorbed on the backside of the pillar against the injection direction. The location of the local oil–water interface in (a) is marked by the solid red line. (b) A representative Janus NP (marked as B) adsorbed on the front side of the pillar facing the injection fluid. Oil molecules migrated with Janus NP in (b) are highlighted in red. Sequential snapshots of the representative NPs over time are given and labeled with T2–5 in both (a) and (b). (For interpretation of the references to colour in this figure legend, the reader is referred to the web version of this article.)

on the backside of the pillars. The results were consistent with observations in experiments [62,63], namely most NPs were found on the backside of the surface rough landscape against injection fluid after displacement. Although the amount of oil carried by the movement of Janus NPs was limited, their associated effect on the trapped oil (extrusion, wettability alteration, and possible structural disjoining pressure) was intriguing. It is reasonable to speculate that in case the geometry of the oil–water interface becomes more abrupt, namely thin oil film covering rougher surface landscape, Janus NPs can be the right choice for their strong interactions with the three-phase contact area and their promising mechanism. Further verification certainly requires more atomistic modeling and experimental studies.

3.2.3. Mechanism by hydrophobic NPs

As discussed above, hydrophobic NPs were likely to enter and stay in the trapped oil phase and yield the lowest displacement efficiency. The occurrence of hydrophobic NPs in trapped oil after the displacement process was summarized in Table 1. Dispersed hydrophobic NPs can be immersed completely in the trapped oil phase or adsorbed on the pillar surface near the oil–water interface. Strikingly, the hydrophobic NPs could also aggregate tightly together in clusters on the solid surface. Due to the similar hydrophobicity, oil molecules also firmly adsorbed on hydrophobic NPs, as snapshots showed in Fig. S7. The average adsorption time of oil molecules on hydrophobic NPs was found to depend on the location of the NPs. For the hydrophobic NPs near the oil–water interface, oil molecules showed a relatively short adsorption time of 0.24 ns. In contrast, oil molecules were closely bound to the hydrophobic NPs immersed in the oil phase for a doubling average time of 0.43 ns. The adsorption time of oil molecules on aggregated NPs clusters was not high (0.29 ns), but when a cluster was taken as the calculation

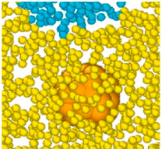
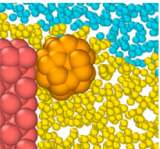
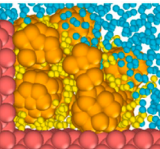
unit, there was a larger value (0.48 ns). Although the flow instability near the oil–water interface can decrease the oil molecule adsorption time, the addition of hydrophobic NPs reduced the mobility of the trapped oil phase, as the atomic velocities of the oil molecules shown in Fig. 4. The formed hydrophobic NP clusters potentially narrowed the flow channel. Slight displacement effect on the trapped oil was only observed close to the inlet region of the channel, owing to the limited volume exclusion effect of the hydrophobic NPs immersed in the trapped oil. For enhancing the displacement effect, a sufficient driving force was needed to separate the bound oil molecules from the hydrophobic NPs and the NP clusters. Furthermore, the hydrophobic NPs had the possibility to form channel blockage, suggesting their application potential in conformance control.

3.3. Effect of the pumping force

The injection pressure, controlled by the pumping force in this work, is known to have a crucial impact on the displacement process [43]. The pumping force was also found to influence the interaction of NPs with the trapped oil here. Although the major features of the final occurrence of NPs after displacement remained similar, increased pumping force can significantly reduce the contact of hydrophobic and Janus NPs with the trapped oil, as shown in Fig. S8. Higher pumping force led to a more obvious displacement effect, which was quantified by the ratio of the number of remaining oil molecules after the displacement to the total amount of the initial state in the channel, termed as EOR percentage in Fig. 7. By sampling pumping force covered two orders of magnitude ranging from 0.00005 to 0.001 kcal/mol/Å, all the injection fluids used in this work yielded a higher EOR percentage with high pumping force. This result was different from the findings on the displacement of oil in

Table 1

Distribution of hydrophobic NPs after displacement processes. Three representative adsorption states are given, with the number of NPs and clusters as well as the adsorption time of oil molecules on the NPs and NP clusters.

State	Immerse deeply in oil	Stay near the surface	Aggregate in clusters
Diagram			
Number	6	5	14(3)
Average adsorption time of oil molecules	0.43 ns	0.24 ns	0.26 ns (0.48 ns)

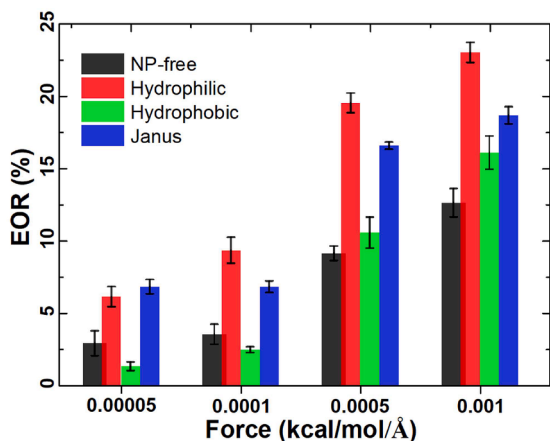


Fig. 7. The EOR percentage by flooding with varied pumping forces.

smooth channels in the previous study [43]. The reason was that the force used in this study was sufficiently low, which guaranteed the stability of the displacing front to achieve piston displacement like in the reservoir. Especially, the oil phase focused here was trapped in the surface roughness landscape of the channel rather than that filled the whole channel. The displacement effect observed relied on the drag at the oil–water interface between the trapped oil and the injection fluids, namely increased external pressure led to enhanced interface squeezing. Because higher pumping force led to shorter displacement time, the probability of NPs contacting with the oil and the solid surface was also reduced. The change in the micro behaviors by hydrophobic and Janus NPs also had a significant impact on the displacement effect. Under higher pumping force, the hydrophobic NPs were more likely to rush through the channel with water instead of sticking into the oil phase (as shown in Fig. S9), which improved the EOR percentage as shown in Fig. 7. Interestingly, as the pumping force at the low level dropping from 0.0001 to 0.00005 kcal/mol/Å, the EOR percentage by Janus NPs remained steady and even surpassed hydrophilic NPs. In the light of the above analysis on Janus NPs, their displacement effect on trapped oil greatly depended on the interactions with the oil and surface. Under the low external force, the elongated displacement time and thus the enhanced contact probability had contributed to the positive impact of Janus NPs on the displacement effect.

The influence of pumping force on displacement effect can also be explained by the well-known capillary number [64]:

$$N_c = \frac{\text{viscous forces}}{\text{capillary forces}} = \frac{v\mu_w}{\sigma_{ow}\cos\theta} \quad (7)$$

where N_c is the capillary number, v is displacing velocity, μ_w is the viscosity of the displacing phase, σ_{ow} is interfacial tension between trapped oil and nanofluids, and θ is the water contact angle. The capillary number reflects the relative range of the driving force and resistance in the oil displacement effects [65] and relates residual oil saturation into three force-dominated regions. As capillary number increases, the residual oil saturation decreases and the three regions of oil displacement in sequence are capillary dominated, viscous-capillary coupling, and viscous dominated. Although the absolute quantitative results can differ under specific reservoir conditions, the qualitative description of the three oil displacement effect regions remains the same [64]. As the pumping force decreases, the displacing rate declines, and the capillary number drops. As a result, the EOR percentage lowers while the dominance of capillary force in the displacement gradually enhances [65,66]. This phenomenon was well reproduced by Janus NPs under low pumping force, as their role in modifying the capillary force gradually became prominent. The results in this work were thus consistent with macroscopic conclusions. More importantly, almost all the reservoirs after water flooding are currently in a viscous-capillary coupling region

or capillary force-dominated region [64,67], which highlights the great EOR application potential for Janus NPs, compared to other types of NPs.

4. Discussion

This study provides nano-level information including the motion patterns of various NPs and the detailed interaction between components in a complex nanofluid system, which is formidable to obtain in large-scale oil displacement experiments. Such findings are essential for deepening the understanding of the mechanisms of EOR by NPs. In order to simulate a sufficiently large system at optimal computational costs, a coarse-grained modeling approach was adopted for the fast sampling dynamics with a reduced degree of freedom of the different components in the system. The selected force field has been proven to successfully reproduce the nature of the components in nanofluid systems [25,42,49,50]. The rough surface was represented by the rectangular groove as in the previous studies [68]. Thus, the designed model is simplified from real rough surfaces but is eligible for trapping a stable oil phase to be displaced by various NPs.

The oil displacement effect obtained by the lowest external force in this work is comparable with results by experiments. Although the Janus NPs are not as good as hydrophilic ones in EOR effect under external force larger than 10^{-4} kcal/mol/Å (Fig. 7), their outperforming oil displacement results at low external force (5×10^{-5} kcal/mol/Å) is striking. According to the previously known effect of the external force on the EOR, the results clearly suggested that the level of the lowest applied force in this work was close to the real conditions, where the EOR effect of Janus gradually became prominent. In other words, Janus NP, with their major oil displacement mechanism that relies on the interactions with both the oil phase and the solid surface, could have great potentials in recovery oil film on rock surfaces in the application.

It is important to note that the oil phase consisting of only hexane used in this work is a simplified model of the real crude oil. The purpose of such an oil phase model is only for the demonstration of the differences in the movement patterns and EOR mechanisms among various NPs. According to the previous studies [69], the polar molecules in crude oil, such as pyridine, asphaltene, prefer to accumulate at fluids interface and solid surface, which leads to the variation of the oil properties and could hinder the efficiency of the oil displacement process. However, the detailed chemical properties of different oil molecules do not counteract the EOR mechanism of different NPs. Nevertheless, considering all the crude oil components in a single study, despite the foreseeable difficulty, could result in a more realistic oil phase in the reservoir, which would be an interesting step in future work. Moreover, only one single channel volume is considered in the work, which could potentially limit the possible contact between the NPs with the oil phase and the solid surface. It is thus highly beneficial to establish cyclic displacement simulation in different channel models for Janus NPs in future work for the in-depth analysis of EOR by nanofluids. Apart from that, water salinity, rock properties, both the size and concentration of NPs, and the system temperature and pressure, still await intensive investigations to establish the systematic theory for nanofluid EOR.

5. Conclusion

This work revealed the displacement mechanisms of trapped oil in the rough channel by injection of nanofluids using MD simulations. The results completed the missing puzzle in the current literature that is dominated by modeling of oil displacement in smooth channels. The study indicated that hydrophilic and Janus NPs were able to drive significantly more trapped oil out of rough channels, while hydrophobic NPs had the lowest potential in trapped oil displacement with endangering probability of channel blockage. Specifically, hydrophilic NPs

dispersed in water increased the viscosity of the injected fluid and disturbed the original stream field. As a result, the friction to the oil phase at the oil–water interface was enhanced and the sweeping scope of the displacing phase was enlarged. Janus NPs adsorbed not only at the oil–water interface to reduce the interfacial tension but also onto the roughness landscape (at two sides of the pillars). Driven by the injected flow, surface wettability, and possible structural disjoining pressure, Janus NPs can migrate along the solid surface and into the trapped oil phase, and further exclude oil out of the trapping pockets and alter the local surface wettability. Moreover, the slippage of Janus NPs at the interface also contributed to the EOR effect. In contrast, hydrophobic NPs dispersed into the oil phase and further formed clusters, showing a negligible displacement effect. Higher pumping force was found to result in better oil displacement in all the systems. It's worth noting that Janus NPs showed outperforming EOR potential with low pumping force. Low force allowed for sufficient contact time between Janus NPs and trapped oil, which was beneficial for the EOR effect. Such phenomena were supported by the analysis of the capillary number, which suggested the EOR application potential of Janus NPs in actual reservoir conditions. The microscopic insights provided by this study are of great importance for the understanding of the oil displacement mechanism of different nanofluids and for the optimization and design of NPs in EOR.

CRedit authorship contribution statement

Yuanhao Chang: Conceptualization, Writing – original draft. **Senbo Xiao:** Methodology, Software. **Rui Ma:** Investigation. **Xiao Wang:** Resources, Investigation. **Zhiliang Zhang:** Supervision. **Jianying He:** Validation, Writing – review & editing.

Declaration of Competing Interest

The authors declare that they have no known competing financial interests or personal relationships that could have appeared to influence the work reported in this paper.

Acknowledgements

This work was financially supported by the Research Council of Norway (Grant No. 234626) and the Chinese Scholarship Council. The supercomputer CPU hours were provided by the Norwegian Metacenter for Computational science (Project ID: NN9110K and NN9391K).

Appendix A. Supplementary data

Supplementary data to this article can be found online at <https://doi.org/10.1016/j.fuel.2021.122760>.

References

- Asif M, Muneer T. Energy supply, its demand and security issues for developed and emerging economies. *Renewable Sustainable Energy Rev* 2007;11(7):1388–413.
- Bradley HB. *Petroleum engineering handbook*. 1987.
- Muggeridge A, et al. Recovery rates, enhanced oil recovery and technological limits. *Philos Trans R Soc A: Math, Phys Eng Sci* 2014;372.
- Lyons WC, Plisga GJ. *Standard handbook of petroleum and natural gas engineering*. Elsevier; 2011.
- Zhang N, et al. Development of a hybrid scoring system for EOR screening by combining conventional screening guidelines and random forest algorithm. *Fuel* 2019;256:115915.
- Shah A, et al. A review of novel techniques for heavy oil and bitumen extraction and upgrading. *Energy Environ Sci* 2010;3(6):700–14.
- Leonard J. Increased rate of EOR brightens outlook. *Oil Gas J*; (United States) 1986;84(15).
- Gurgel A, et al. A review on chemical flooding methods applied in enhanced oil recovery. *Braz J Petrol Gas* 2008;2(2).
- Sun X, et al. Enhanced heavy oil recovery in thin reservoirs using foamy oil-assisted methane huff-n-puff method. *Fuel* 2015;159:962–73.
- Rezk MY, Allam NK. Impact of nanotechnology on enhanced oil recovery: a mini-review. *Ind Eng Chem Res* 2019;58(36):16287–95.
- Haruna MA, et al. Nanoparticle modified polyacrylamide for enhanced oil recovery at harsh conditions. *Fuel* 2020;268:117186.
- Sun Y, et al. Properties of nanofluids and their applications in enhanced oil recovery: a comprehensive review. *Energy Fuels* 2020;34(2):1202–18.
- Alnarabiji MS, Husein MM. Application of bare nanoparticle-based nanofluids in enhanced oil recovery. *Fuel* 2020;267:117262.
- Murshed SS, De Castro CN. *Nanofluids: synthesis, properties, and applications*. Nova Science Publishers, Incorporated; 2014.
- Nowrouzi I, Manshad AK, Mohammadi AH. Effects of TiO₂, MgO, and γ -Al₂O₃ nano-particles in carbonated water on water-oil interfacial tension (IFT) reduction in chemical enhanced oil recovery (CEOR) process. *J Mol Liq* 2019;292:111348.
- Al-Anssari S, et al. Effect of temperature and SiO₂ nanoparticle size on wettability alteration of oil-wet calcite. *Fuel* 2017;206:34–42.
- Adil M, Zaid HM, Chuan LK. Electromagnetically-induced change in interfacial tension and contact angle of oil droplet using dielectric nanofluids. *Fuel* 2020;259:116274.
- Hendraningrat L, Li S, Torsæter O. A coreflood investigation of nanofluid enhanced oil recovery. *J Petrol Sci Eng* 2013;111:128–38.
- Moldoveanu GM, et al. Experimental study on viscosity of stabilized Al₂O₃, TiO₂ nanofluids and their hybrid. *Thermochim Acta* 2018;659:203–12.
- Nabil M, et al. An experimental study on the thermal conductivity and dynamic viscosity of TiO₂-SiO₂ nanofluids in water: ethylene glycol mixture. *Int Commun Heat Mass Transfer* 2017;86:181–9.
- Sun X, et al. Application of nanoparticles in enhanced oil recovery: a critical review of recent progress. *Energies* 2017;10(3):345.
- Wasan D, Nikolov A, Kondiparty K. The wetting and spreading of nanofluids on solids: Role of the structural disjoining pressure. *Curr Opin Colloid Interface Sci* 2011;16(4):344–9.
- Wasan DT, Nikolov AD. Spreading of nanofluids on solids. *Nature* 2003;423(6936):156–9.
- Zhang H, Nikolov A, Wasan D. Dewetting film dynamics inside a capillary using a micellar nanofluid. *Langmuir* 2014;30(31):9430–5.
- Chang Y, et al. Nanomechanical characteristics of trapped oil droplets with nanoparticles: a molecular dynamics simulation. *J Petrol Sci Eng* 2021;203:108649.
- Yakasai F, et al. Current developments and future outlook in nanofluid flooding: a comprehensive review of various parameters influencing oil recovery mechanisms. *J Ind Eng Chem* 2020.
- Sedghi M, Piri M, Goual L. Atomistic molecular dynamics simulations of crude oil/brine displacement in calcite mesopores. *Langmuir* 2016;32(14):3375–84.
- Li C, Li Y, Pu H. Molecular simulation study of interfacial tension reduction and oil detachment in nanochannels by surface-modified silica nanoparticles. *Fuel* 2021;292:120318.
- Zhao J, et al. Molecular dynamics investigation of substrate wettability alteration and oil transport in a calcite nanopore. *Fuel* 2019;239:1149–61.
- Ahmadi M, Chen Z. Comprehensive molecular scale modeling of anionic surfactant-asphaltene interactions. *Fuel* 2021;288:119729.
- Ahmadi M, Chen Z. Spotlight onto surfactant–steam–bitumen interfacial behavior via molecular dynamics simulation. *Sci Rep* 2021;11(1):1–33.
- Ahmadi M, et al. Interfacial and molecular interactions between fractions of heavy oil and surfactants in porous media: comprehensive review. *Adv Colloid Interface Sci* 2020:102242.
- Ahmadi M, Chen Z. Molecular interactions between asphaltene and surfactants in a hydrocarbon solvent: application to asphaltene dispersion. *Symmetry* 2020;12(11):1767.
- Ahmadi M, Chen Z. Insight into the interfacial behavior of surfactants and asphaltenes: molecular dynamics simulation study. *Energy Fuels* 2020;34(11):13536–51.
- Miranda CR, Lara LSd, Tonetto BC. Stability and mobility of functionalized silica nanoparticles for enhanced oil recovery applications. *SPE international oilfield nanotechnology conference and exhibition*. Society of Petroleum Engineers; 2012.
- Fan H, Striolo A. Nanoparticle effects on the water-oil interfacial tension. *Phys Rev E* 2012;86(5):051610.
- de Lara LS, Rigo VA, Miranda CR. Functionalized silica nanoparticles within multicomponent oil/brine interfaces: a study in molecular dynamics. *J f Phys Chem C* 2016;120(12):6787–95.
- Wu J, et al. Effect of nanoparticles on oil-water flow in a confined nanochannel: a molecular dynamics study. *SPE international oilfield nanotechnology conference and exhibition*. Society of Petroleum Engineers; 2012.
- Wang F, Wu H. Molecular dynamics studies on spreading of nanofluids promoted by nanoparticle adsorption on solid surface. *Theor Appl Mech Lett* 2013;3(5).
- Wang F-C, Wu H-A. Enhanced oil droplet detachment from solid surfaces in charged nanoparticle suspensions. *Soft Matter* 2013;9(33).
- Wang X, et al. Atomistic insights into the nanofluid transport through an ultra-confined capillary. *Phys Chem Chem Phys* 2018;20(7):4831–9.
- Wang X, et al. Transportation of Janus nanoparticles in confined nanochannels: a molecular dynamics simulation. *Environ Sci Nano* 2019;6(9):2810–9.
- Wang X, et al. Insight into the pressure-induced displacement mechanism for selecting efficient nanofluids in various capillaries. *Environ Sci Nano* 2020;7(9):2785–94.
- Durret J, et al. Superhydrophobic polymeric films with hierarchical structures produced by nanoimprint (NIL) and plasma roughening. *Appl Surf Sci* 2018;445:97–106.
- Savoy ES, Escobedo FA. Molecular simulations of wetting of a rough surface by an oily fluid: effect of topology, chemistry, and droplet size on wetting transition rates. *Langmuir* 2012;28(7):3412–9.

- [46] Wang G, et al. Kinetic Monte Carlo study on the evolution of silicon surface roughness under hydrogen thermal treatment. *Appl Surf Sci* 2017;414:361–4.
- [47] Meng Q, Chen D, Wu G. Microscopic Mechanisms for the dynamic wetting of a heavy oil mixture on a rough silica surface. *J Phys Chem C* 2018;122(43):24977–86.
- [48] Moulton OA, et al. Atomistic molecular dynamics simulations of carbon dioxide diffusivity in n-hexane, n-decane, n-hexadecane, cyclohexane, and squalane. *J Phys Chem B* 2016;120(50):12890–900.
- [49] Molinero V, Moore EB. Water modeled as an intermediate element between carbon and silicon. *J Phys Chem B* 2009;113(13):4008–16.
- [50] Martin MG, Siepmann JL. Transferable potentials for phase equilibria. 1. United-atom description of n-alkanes. *J Phys Chem B* 1998;102(14):2569–77.
- [51] Plimpton S. Fast parallel algorithms for short-range molecular dynamics. Sandia National Labs. Albuquerque, NM (United States); 1993.
- [52] Stillinger FH, Weber TA. Computer simulation of local order in condensed phases of silicon. *Phys Rev B* 1985;31(8):5262.
- [53] Hoover WG. Canonical dynamics: equilibrium phase-space distributions. *Phys Rev A* 1985;31(3):1695.
- [54] Nosé S. A unified formulation of the constant temperature molecular dynamics methods. *J Chem Phys* 1984;81(1):511–9.
- [55] Stukowski A. Visualization and analysis of atomistic simulation data with OVITO—the Open Visualization Tool. *Modell Simul Mater Sci Eng* 2009;18(1):015012.
- [56] Willhite GP. *Waterflooding*; 1986.
- [57] Craig FF. The reservoir engineering aspects of waterflooding. HL Doherty Memorial Fund of AIME New York; 1971.
- [58] Thomas JA, McGaughey AJ. Reassessing fast water transport through carbon nanotubes. *Nano Lett* 2008;8(9):2788–93.
- [59] Speight JG. *Introduction to enhanced recovery methods for heavy oil and tar sands*. Gulf Professional Publishing; 2016.
- [60] Giraldo LJ. Janus nanoparticles for enhanced oil recovery EOR: Reduction of Interfacial Tension. SPE annual technical conference and exhibition. Society of Petroleum Engineers; 2018.
- [61] Eltoun H, Yang Y-L, Hou J-R. The effect of nanoparticles on reservoir wettability alteration: a critical review. *Pet Sci* 2020;18(1):136–53.
- [62] Chang B, et al. Sliding droplets on hydrophilic/superhydrophobic patterned surfaces for liquid deposition. *Appl Phys Lett* 2016;108(15).
- [63] Zhang P, et al. Grooved organogel surfaces towards anisotropic sliding of water droplets. *Adv Mater* 2014;26(19):3131–5.
- [64] Guo H, Song K, Hilfer R. A critical review of capillary number and its application in enhanced oil recovery. SPE improved oil recovery conference. Society of Petroleum Engineers; 2020.
- [65] Guo H, et al. Review of capillary number in chemical enhanced oil recovery. SPE Kuwait Oil and Gas Show and Conference. Society of Petroleum Engineers; 2015.
- [66] Yiotis A, et al. Pore-scale effects during the transition from capillary-to viscosity-dominated flow dynamics within microfluidic porous-like domains. *Sci Rep* 2021; 11(1):1–16.
- [67] Masalmeh SK. Impact of capillary forces on residual oil saturation and flooding experiments for mixed to oil-wet carbonate reservoirs. SCA. 2012.
- [68] Fang T, et al. Oil extraction mechanism in CO₂ flooding from rough surface: Molecular dynamics simulation. *Appl Surf Sci* 2019;494:80–6.
- [69] Wang X, et al. Displacement of nanofluids in silica nanopores: influenced by wettability of nanoparticles and oil components. *Environ Sci Nano* 2018;5(11):2641–50.